Pflugers Arch - Eur J Physiol (2014) 466:1391–1409
DOI 10.1007/s00424-013-1382-1

ION CHANNELS, RECEPTORS AND TRANSPORTERS

# TMEM16A knockdown abrogates two different $Ca^{2+}$-activated $Cl^-$ currents and contractility of smooth muscle in rat mesenteric small arteries

**Vibeke Secher Dam · Donna M. B. Boedtkjer · Jakob Nyvad · Christian Aalkjaer · Vladimir Matchkov**

Received: 9 August 2013 / Revised: 10 October 2013 / Accepted: 10 October 2013 / Published online: 27 October 2013


**Abstract** The presence of $Ca^{2+}$-activated $Cl^-$ channels (CaCCs) in vascular smooth muscle cells (SMCs) is well established. Their molecular identity is, however, elusive. Two distinct $Ca^{2+}$-activated $Cl^-$ currents ($I_{Cl(Ca)}$) were previously characterized in SMCs. We have shown that the cGMP-dependent $I_{Cl(Ca)}$ depends on bestrophin expression, while the "classical" $I_{Cl(Ca)}$ is not. Downregulation of bestrophins did not affect arterial contraction but inhibited the rhythmic contractions, vasomotion. In this study, we have used in vivo siRNA transfection of rat mesenteric small arteries to investigate the role of a putative CaCC, TMEM16A. Isometric force, $[Ca^{2+}]_i$, and SMC membrane potential were measured in isolated arterial segments. $I_{Cl(Ca)}$ and GTPγS-induced nonselective cation current were measured in isolated SMCs. Downregulation of TMEM16A resulted in inhibition of both the cGMP-dependent $I_{Cl(Ca)}$ and the "classical" $I_{Cl(Ca)}$ in SMCs. TMEM16A downregulation also reduced expression of bestrophins. TMEM16A downregulation suppressed vasomotion both in vivo and in vitro. Downregulation of TMEM16A reduced agonist (noradrenaline and vasopressin) and $K^+$-induced contractions. In accordance with the depolarizing role of CaCCs, TMEM16A downregulation suppressed agonist-induced depolarization and elevation in $[Ca^{2+}]_i$. Surprisingly, $K^+$-induced depolarization was unchanged but $Ca^{2+}$ entry was reduced. We suggested that this is due to reduced expression of the L-type $Ca^{2+}$ channels, as observed at the mRNA level. Thus, the importance of TMEM16A for contraction is, at least in part, independent from membrane potential. This study demonstrates the significance of TMEM16A for two SMCs $I_{Cl(Ca)}$ and vascular function and suggests an interaction between TMEM16A and L-type $Ca^{2+}$ channels.

**Keywords** $Ca^{2+}$-activated $Cl^-$ channel · Excitation–contraction coupling · Smooth muscle cells · siRNA · Membrane potential · Intracellular calcium

V. S. Dam · D. M. B. Boedtkjer · J. Nyvad · C. Aalkjaer · V. Matchkov (✉)
Department of Biomedicine, MEMBRANES, Aarhus University, Ole Worms Alle bygn.4, 1163, Aarhus C 8000, Denmark
e-mail: vvm@fi.au.dk

## Introduction

Calcium-activated chloride channels (CaCCs) have been intensely studied during the last decade [16]. This is, in part, because these channels represent the largest remaining group of membrane conductances for which the molecular identity is uncertain [40]. Recent functional and structural studies strengthen though the position of the TMEM16 family (anoctamins), which are one of the most prominent candidates for CaCCs [13, 15, 16, 20]. The heterologous overexpression of at least some members of the TMEM16 family, i.e., TMEM16A and TMEM16B, induces a $I_{Cl(Ca)}$ with characteristics closely resembling the properties of the endogenous $I_{Cl(Ca)}$ in smooth muscle cells (SMCs) [5, 43, 47]. Moreover, it has been shown that native $I_{Cl(Ca)}$ depends on TMEM16A expression [1, 8, 17, 24, 44]. Genetic knockout or ex vivo siRNA-based downregulation of TMEM16A suppresses native $I_{Cl(Ca)}$ and abolishes some CaCC-dependent cellular functions [16, 20].

The presence of CaCCs in SMCs is well established [22, 23]. The SMC $I_{Cl(Ca)}$ is well characterized and its functional significance documented. Since $Cl^-$ is actively transported into SMCs, increased SMC $Cl^-$ current depolarizes the cell membrane [6] and $I_{Cl(Ca)}$ has been suggested to participate in excitation–contraction coupling. Agonist-induced $Ca^{2+}$ release

is generally thought to lead to CaCC-dependent membrane depolarization which in turn opens voltage-gated $Ca^{2+}$ channels, which further increases the intracellular $Ca^{2+}$. The native $I_{Cl(Ca)}$ has also been suggested to be important for SMC proliferation during vascular remodeling and for mechanosensitive responses of the arterial wall [46]. Recently, TMEM16A has been shown to be important for $I_{Cl(Ca)}$, for membrane potential, and for myogenic tone in rat cerebral arteries [4].

We have previously shown that vascular SMC $I_{Cl(Ca)}$ is comprised of two currents [25]: in addition to the $I_{Cl(Ca)}$ with classical biophysical and pharmacological characteristics [25, 27], we identified a cGMP-dependent $I_{Cl(Ca)}$ in the same SMCs. The two $Cl^-$ currents co-exist throughout the vascular tree, although the relative expression differs between vascular beds [26]. Interestingly, pulmonary arteries exhibit no cGMP-dependent $I_{Cl(Ca)}$ [25, 26]. Using siRNA, we have previously demonstrated that knockdown of bestrophin expression is associated with disappearance of the cGMP-dependent $I_{Cl(Ca)}$ in SMCs [27] but has no effect on the "classical" $I_{Cl(Ca)}$. We also found that knockdown of bestrophin is not important for agonist-induced contraction [3]. This is consistent with other studies showing that the $Cl^-$ gradient is not important for agonist-induced vasoconstriction of rat mesenteric arteries [2]. A key role for $I_{Cl(Ca)}$ in contraction is suggested in other species and vascular beds, e.g., rabbit mesenteric arteries, although the ion substitution experiments were not performed there [41]. Thus, the exact role of the "classical" $I_{Cl(Ca)}$ for SMC agonist-induced contraction remains unclear. However, downregulation of bestrophins significantly suppresses vasomotion [3], which supports the hypothesis that the cGMP-dependent $I_{Cl(Ca)}$ is important for synchronization of SMCs in the generation of vasomotion [37].

In this study, we test the hypothesis that TMEM16A, which is endogenously expressed in SMCs [8, 24, 44], is necessary for the native $I_{Cl(Ca)}$: to do so, we downregulated TMEM16A in rat mesenteric small arteries in vivo with siRNA [3, 27, 28]. We found that the presence of TMEM16A is important for both the cGMP-independent $I_{Cl(Ca)}$ and the cGMP-dependent $I_{Cl(Ca)}$. The interpretation of this result is complicated, however, by our finding that downregulation of TMEM16A leads to reduced expression of bestrophins, which previously has been shown to be important for the cGMP-dependent $I_{Cl(Ca)}$ [27]. Furthermore, downregulation of TMEM16A reduced the contractile response and inhibited vasomotion. Elevations in intracellular $Ca^{2+}$ and membrane potential in response to agonist stimulation were also reduced in TMEM16A-downregulated arteries. However, the contractile response to $K^+$-induced depolarization was also reduced and this was accompanied by a reduced expression of vascular voltage-dependent L-type $Ca^{2+}$ channels. The current study suggests that TMEM16A is important for SMCs contraction in membrane potential-dependent and potential-independent ways.

## Methods

All experiments were approved by and conducted with permission from the Animal Experiments Inspectorate of the Danish Ministry of Justice.

### In vivo siRNA transfection

A segment of rat mesenteric small arteries was transfected in vivo as described previously [3, 28]. Shortly, Wistar male rats were anesthetized with a subcutaneous injection of a combination of Hypnorm (1 mg/100 g; VetaPharma Ltd., UK) and midazolam (0.5 mg/100 g; Hameln Pharm GMBH, Germany). Supplementary anesthesia was given each half hour during the transfection procedure. A medial laparotomy was performed and a section of the mesentery was gently pulled out. A short segment (~1 mm) of a first order branch from the superior mesenteric artery was gently cleaned of fat and the tip (~0.5 mm length) of an elastic micropipette (MicroFill 34G-5; World Precision Instruments Inc., USA) was inserted through a puncture made by a needle. The downstream arteries were flushed with the transfection solution and a clamp was placed near the entrance of the small arteries to the gut wall to avoid backflow of blood from the mesenteric arcade; care was taken to avoid overfilling of the artery segments. Transfection was performed for 20 min; every 2.5 min, the downstream clamp was released and the arteries flushed with new transfection solution. After transfection, the mesentery was returned to the peritoneal cavity and the wound closed. The painkiller Temgesic® (2 mL/100 g; Schering-Plough, Belgium) was given at the end of the transfection.

TKO®-based transfection was used (Mirus Bio Co., USA). The concentration of siRNA in the final transfection solution was ~800 nM. The siRNA oligos were manufactured by Eurofin MWG Operon (Germany) with TT overhang (Table 1), and the efficiency of siRNA transfection was initially tested on a smooth muscle cell line (A7r5) (not shown). Two different siRNA directed against *Tmem16a* were used in the study (Table 1): one was directed against exon 23 (*Tmem16a*-siRNA) and was used throughout the whole study, while the second was directed against exon 22 (*Tmem16a*-siRNA-2) and was used in some experiments. Two mesenteric artery branches from one rat were transfected each time; one with siRNA directed against *Tmem16a* and another with control siRNA. Either nonrelated siRNA directed against enhanced green fluorescent protein (eGFP; Ambion Ltd) or nonfunctional siRNA directed against *Tmem16a* with four mutated nucleotides was used as the control siRNA (Table 1).

Three days after transfection, rats were either used for in vivo study or sacrificed by $CO_2$ inhalation to permit mesenteric arteries to be harvested for in vitro studies. Arteries transfected with *Tmem16a*-siRNA, arteries

**Table 1** Oligonucleotide sequences

| Primer (sequencing experiments) | Sequence | Target |
|---|---|---|
| rTM_47-66 F | catcatgcaggacacacagg | Bp 47–[a] |
| rTM_751-770 F | tgcccacgaagaaggtgtac | Bp 751–[a] |
| rTM_1555-1574 F | ccttcatggagcactggaaa | Bp 1555–[a] |
| rTM_1861-1880 F | tgaactcctccccatctgtg | Bp 1861–[a] |
| rTM_2540-2559 F | agccatcagagccaaagaca | Bp 2540–[a] |
| rTM_3361-3380 F | aggccattatgcagggaagt | Bp 3361–[a] |
| rTM_747-766R | accttcttcgtgggcatctt | Bp −766[a] |
| rTM_1054-1073R | cgccgtttacttagaagggc | Bp −1073[a] |
| rTM_1861-1880R | cacagatggggaggagttca | Bp −1880[a] |
| rTM_3090-3109R | ctgtgggactgtggttgtta | Bp −3109[a] |
| rTM_3694-3713R | ccaggcttatttctgaccct | Bp −3713[a] |
| rTM_4600-4619R | gaacgctcagccacagactc | Bp −4619[a] |
| siRNA | Sequence | |
| *Tmem16a*-siRNA (exon 23) | cggucuucuuucuucuuucTT | Ano1/NM_001107564.1[b] |
| mutated *Tmem16a*-siRNA | cggucggcuuacaucuuucTT | Ano1/NM_001107564.1[b] |
| *Tmem16a*-siRNA-2 (exon 22) | guuuuuaucuuuaguauucTT | Ano1/NM_001107564.1[b] |
| eGFP-siRNA | ccacuaccugagcacccagTT | eGFP[b] |
| Primer (qPCR) | Sequence | |
| rTM_taq2621-F | tgtgatctccttcacgtctg | Ano1/NM_001107564.1[b] |
| rTM_taq2825-R | catacttgtgttctgaccacg | Ano1/NM_001107564.1[b] |
| rCacna1c-F | catctccatcaccttcttccg | Cacna1c/NM_012517.2[b] |
| rCacna1c-R | aaatacctgcatcccaatcactg | Cacna1c/NM_012517.2[b] |
| α1a α-adrenergic receptors-F | ccgttcttcctagtcatgcc | Adra1a/NM_0171981.2[b] |
| α1a α-adrenergic receptors-R | atgtctctgtgctgtccctc | Adra1a/NM_017191.2[b] |
| α1b α-adrenergic receptors-F | caagaactttcatgaggacaccc | Adra1b/NM_016991.2[b] |
| α1b α-adrenergic receptors-R | ccagaacaccaccttgaacac | Adra1b/NM_016991.2[b] |
| α1d α-adrenergic receptors-F | cggaccacagagtagcaagg | Adra1d/NM_024483.1[b] |
| α1d α-adrenergic receptors-R | tagcccagccagaagatgac | Adra1d/NM_024483.1[b] |
| rBest1 (Applied Biosystems) | Rn01451107_m1 | Best1/NM_001011940.1[b] |
| rBest2 (Applied Biosystems) | Rn00520372_m1 | Best2/NM_001108895.1[b] |
| rBest3 (Applied Biosystems) | Rn01509681_m1 | Best3/NM_001191783.1[b] |
| rGAPDH_taq1000-F | cacggcaagttcaacggcacag | Gapdh/NM_017008.3[b] |
| rGAPDH_taq1138-R | agactccacgacatactcagcacc | Gapdh/NM_017008.3[b] |
| rTfrc_taq1708-F | agacagtaattggattagcaaaattg | Tfrc/NM_022712.1[b] |
| rTfrc_taq1961-R | gggtcaactcaatgtcatgggta | Tfrc/NM_022712.1[b] |
| Probe | Sequence | |
| rTM_taq2690-P | acctctacatgtacagtcaaaacgggacc | Ano1/NM_001107564.1[b] |
| Rcacna1c-P | tgctgtggaccttcatcaagtccttccagg | Cacna1c/NM_012517.2[b] |
| rGAPDH_taq1040-P | agctggtcatcaacgggaaacccatcacca | Gapdh/NM_017008.3[b] |
| rTfrc_taq1905-P | cagcagaggtggccggtcagttcattattaaa | Tfrc/NM_022712.1[b] |

[a] Target position

[b] Target gene

transfected with control siRNA (either eGFP-siRNA or mutated *Tmem16a*-siRNA), and nontransfected arteries from the same rat were used for the following studies.

## Contractile responses of mesenteric small arteries in vivo

Three days after transfection, rats were anesthetized using ketamine (33 mg/100 g; Ketaminol®vet, Intervet International, Holland) and xylazine (7.5 mg/100 g; Narcoxyl®vet, Intervet International, Holland) administered subcutaneously and placed in a chamber heated to 33–37 °C. A lateral laparotomy was performed and a short segment (1.5–2 cm) of the intestine and mesentery were carefully pulled out. A single branch of the mesenteric artery was placed in a small reservoir (6.5 mm width × 6.5 mm length × 3 mm depth, corresponding to a volume of ~100 μL) by passing ends of the branch through openings at

the two sides of the reservoir. The openings between the reservoir walls and the artery were sealed with high vacuum grease (Dow Corning GMBH, Wiesbaden, Germany). Thus, the mesenteric artery segment in the reservoir was perfused but isolated extraluminary from the rest of intestine and mesentery. The reservoir was filled with physiological saline solution (PSS) containing 10 mM HEPES (HEPES-PSS) bubbled with 5 % $CO_2$ in $N_2$. During the experiment, the extracted intestine and mesentery were kept moist using bandages soaked in HEPES-PSS. Different noradrenaline (NA) concentrations were applied by adding 10 μL corresponding stock solution prepared in HEPES-PSS to the reservoir. Each concentration was applied for 2–3 min.

The rat was placed on a microscope (Motic PSM-1000) table and the artery was focused. Approximately 50 % of the surrounding mesenteric fat was dissected from the top of the segment to enable visualization of the inner diameter of the artery. The arterial inner diameter was captured with a USB CCD Monochrome Camera (DMK 41 AU02, Imaging Source, Germany) attached to the microscope and processed using DMT Vessel Acquisition Suite software (Danish Myo Technology A/S, Denmark). The diameter measured immediately after washout three times was not different from the passive diameter measured in vivo in the presence of 10 μM papaverine hydrochloride, 1 μM phentolamine, 10 μM Y-27632, and 10 μM acetylcholine (data not shown). Therefore, changes in vascular tone are expressed as a percent reduction of the passive (washout) diameter.

### mRNA quantification—quantitative polymerase chain reaction (qPCR)

Arteries were dissected and stored in stabilizing reagent RNA*later* (Qiagen, VWR, Denmark). Isolated arterial segments were homogenized in Tissue Lyser (0.033 Hz; Qiagen, VWR, Denmark) for 3 min. RNA isolation was carried out using RNeasy Micro kit (Qiagen, VWR, Denmark) according to the manufacturer's protocol, followed by standard reverse transcriptase. Quantitative PCR (qPCR) was performed to assess the expression of specific RNAs (Table 1) using Taqman probe technology (*Tmem16a* mRNA quantification; Eurofins MWG Operon, Germany and *bestrophin* mRNA quantification; Applied Biosystems, Denmark) with the amplified sequence being different from the siRNA-targeted sequence. Quantification of RNA for α1a, α1b, and α1d adrenergic receptors was performed using a SYBR Green assay. All amplifications were carried out on MX3000P (Stratagene, USA). Gene expression was normalized to GAPDH and transferrin receptor expression (average Ct value) and presented as a ΔCt value. Comparison of gene expression between nontransfected control and transfected arteries was derived by subtracting control ΔCt from the transfected ΔCt value, producing ΔΔCt. Relative gene expression was calculated as $1/(2^{\Delta\Delta Ct})$, thereby standardizing the data to the nontransfected control arteries from the same rat.

### Analyses of *Tmem16a* splice variants

Primers used for amplification of different fragments of *Tmem16a* are listed in Table 1. The PCR products obtained from rat mesenteric artery and aorta cDNA were sequenced (Eurofins MWG Operon, Germany) and aligned with the predicted mRNA sequence using CLC bio-software (CLC bio, Denmark).

### Quantification of TMEM16A protein expression—single-cell immunofluorescence

Single SMCs for single-cell immunofluorescence and voltage-clamp studies were isolated from rat mesenteric small arteries as described previously [25]. Briefly, artery segments were dissected out, opened longitudinally, and placed in a papain digestion solution at 4 °C overnight. The papain digestion solution contained the following (in mM): NaCl 110, KCl 5, $MgCl_2$ 2, $KH_2PO_4$ 0.5, $NaH_2PO_4$ 0.5, $NaHCO_3$ 10, $CaCl_2$ 0.16, EDTA 0.49, Na-HEPES 10, glucose 10, taurine 10, as well as 1.5 mg/mL papain, 1.6 mg/mL albumin, and 0.4 mg/mL dl-dithiothreitol; pH was adjusted to 7.0. Digestion was completed the next morning by heating the sample to 37 °C for 2–5 min. Single cells were released by trituration with a polyethylene pipette.

The single SMCs were fixated with 4 % formaldehyde (in phosphate-buffered solution (PBS)) for 15 min. After washing, unreacted fixative was quenched with 25 mM glycine in PBS and cells were permeabilized with 0.1 % Triton-X in PBS. Subsequently, the cells were incubated with 0.1 % Triton-X in PBS solution containing the primary antibody raised against TMEM16A (prediluted ab53213 antibody, Abcam, UK) for 2 h at room temperature. The cells were then washed and incubated in the dark with Alexa Fluor 488-conjugated secondary antibody for 45 min at room temperature (Invitrogen, USA). After washing, the preparation was transferred to the confocal microscope.

After excitation at 488 nm, the emission signal (LP 530 nm) was recorded and stored on the computer for later analyses of fluorescence intensity using ImageJ (NIH, USA). All recordings were made with the same microscope settings. No staining was detected in preparations treated with only secondary antibody without primary antibody (not shown). The intensity of TMEM16A-downregulated SMCs was normalized to the level in cells isolated from arteries transfected with eGFP-siRNA.

### Voltage-clamp recordings of membrane currents

All experiments were made at room temperature (22–24 °C). Patch pipettes were prepared from borosilicate glass (PG15OT-7.5; Harvard Apparatus), pulled on a P-97 puller (Sutter Instrument Co.) and fire-polished to achieve tip resistances in the range of 5–10 MΩ. Recordings were made with an Axopatch 200B amplifier (Axon Instruments, Inc.) in whole-cell configuration as described previously [25, 27]. Data were sampled at a rate of 2 kHz and filtered at 1 kHz. Data acquisition and analysis were done with the software package Clampex 7 for Windows (Axon Instruments, Inc.). Series resistance and capacitive current were routinely compensated.

$Ca^{2+}$-activated $Cl^-$ currents were measured at a holding potential of −60 mV. The $Ca^{2+}$-activated currents were evoked by patch pipette solution containing the following (in mM): 140 CsCl, 5.5 $Ca(OH)_2$, 0.1 MgATP, 6 EGTA, and 10 HEPES, at pH 7.35 (free calcium concentration 900 nM, estimated using WEBMAXC v. 2.22 (Chris Patton, Stanford University, USA)) [27]. The bath solution contained the following (in mM): 140 CsCl, 0.1 $CaCl_2$, and 10 HEPES, at pH 7.4. In accordance with our previous findings [25, 26], 1 mM $BaCl_2$ and 100 nM charybdotoxin were included in all bath solutions to prevent the activation of outward current by niflumic acid [14]. The current–voltage ($I$–$V$) relationship was determined by stepping the potentials (20 mV increments) between −60 and +60 mV, maintaining the voltage at each step for 1,500 ms. Sustained current amplitudes were averaged for each step.

We compared the cGMP-dependent and the cGMP-independent $Ca^{2+}$-activated $Cl^-$ currents from the same cells based on differences in their characteristics [25–27]: 100 μM niflumic acid, 300 μM of the membrane-permeable cGMP analog 8Br-cGMP, and 10 μM $Zn^{2+}$ were used as indicated to characterize the currents. We isolated the niflumic acid-sensitive cGMP-independent $Ca^{2+}$-activated $Cl^-$ current and the cGMP-dependent $Ca^{2+}$-activated $Cl^-$ current by subtractions of the current after application of inhibitor (niflumic acid and $ZnCl_2$, respectively) from the current before these agents were added [26]. Currents were normalized to cell capacitances. The current slope conductances were evaluated as the slope of the $I$–$V$ relationship of corresponding current.

Nonselective cationic current ($I_{NSC}$) was recorded as described elsewhere [32]. SMCs were isolated by papain digestion and bathed in the solution containing the following (in mM): 126 NaCl, 6 KCl, 2 $CaCl_2$, 1.2 $MgCl_2$, 14 glucose, and 10.5 HEPES, pH adjusted to 7.2 with NaOH. Before $I_{NSC}$ recording, this bath solution was replaced with a $Cs^+$-rich solution containing the following (in mM): 120 CsCl, 12 glucose, and 10 HEPES, pH adjusted to 7.2 with CsOH. The pipette solution SMCs were dialyzed to evoke $I_{NSC}$ current which contained the following (in mM): 80 CsCl, 1 MgATP, 1 $Na_2GTP$, 5 creatinine, 20 glucose, 10 HEPES, 10 BAPTA (1,2-*bis*(2-aminophenoxy)-ethane-*N*,*N*,*N*′,*N*′-tetraacetic acid), and 4.6 $CaCl_2$ (free $[Ca^{2+}]_i$ estimated to 100 nM), pH adjusted to 7.2 with CsOH.

Upon formation of a whole cell, the membrane voltage was held at −50 mV and the changes in membrane current were recorded. The current–voltage ($I$–$V$) relationship was determined by 200 ms voltage ramp from −90 to +90 mV. The ramp was repeated every 10 s. $I_{NSC}$ was evoked by dialyzing SMCs with 400 μM GTPγS in the pipette solution as described previously [32]. Omission of GTPγS from the pipette solution (not shown) prevents $I_{NSC}$ development. At the end of the experiment, $I_{NSC}$ was inhibited by 10 μM $GdCl_3$.

### Isometric force

Transfected or nontreated second to third order segments of the mesenteric artery were dissected out and cleaned of connective tissue in ice-cold salt solution (PSS). The cleaned arterial segments were mounted in an isometric wire myograph (Danish Myo Technology A/S, Denmark) as described previously [2, 3]. The myograph chamber was heated to 37 °C, while the PSS was constantly aerated with 5 % $CO_2$ in air. Force was recorded with a PowerLab 4/25 and Chart7 data acquisition system (ADInstruments Ltd., New Zealand) and converted to wall tension by dividing force with double segment length. Concentration–response relationships were constructed by cumulative NA (0.1–30 μM) or arginine vasopressin (AVP, 0.15–15 nM) addition. Additionally, the response to 10 mM caffeine and 124 mM $K^+$ was tested.

Vasomotion was analyzed at the level of NA tone where the amplitude was highest, i.e., approximately 50 % of maximal tone [3] for both the in vitro and the in vivo experiments. Vasomotion was analyzed in Chart7 (ADInstruments Ltd., New Zealand) by spectrum analysis.

### Simultaneous measurements of isometric force and intracellular calcium

Simultaneous measurements of isometric force and intracellular $Ca^{2+}$ were performed as described previously [28, 29]. Arteries in the isometric myograph were loaded with 2.5 μM Fura-2 (Fura-2, AM; Invitrogen) in a loading buffer (final bath concentration 0.04 % DMSO, 0.0016 % pluronic F127, 0.008 % Cremophor EL) for two consecutive 30-min periods at 37 °C. Fura-2-loaded preparations were investigated on the stage of an Olympus IX70 microscope equipped with an Olympus LUCPlanFL N×20 objective (N.A. 0.45) and an EasyRatioPro fluorescence imaging system (Photon Technology International, NJ, USA). The arteries in the isometric myograph were exited at 340 and 380 nm and

emission was recorded at 510 nM. Concentration–response relationships were constructed by cumulative NA (0.1–30 μM) addition to the myograph bath. Responses to 10 mM caffeine and 60 mM $K^+$ were tested. $K^+$ response was performed after pre-incubation with 1 μM phentolamine. At the end of the experiment, the $K^+$ response was recorded after incubation with 10 μM nifedipine. Background fluorescence (after quenching with 20 mM $MnCl_2$) was determined at the end of each experiment and subtracted. Intracellular $Ca^{2+}$ ($[Ca^{2+}]_i$) was expressed from 340/380 fluorescence ratio, normalized to mean 340/380 fluorescence ratio in eGFP-transfected arteries in the presence of 10 μM NA.

### Membrane potential

The arterial segments were mounted as described above in the isometric myograph. Intracellular recordings of membrane potential were obtained using glass KCl-filled microelectrodes with resistance in the range of 40–100 MΩ as previously described [29]. A reference electrode (Ag–AgCl) was placed in the myograph bath. Electrode resistance was routinely compensated by balancing the Wheatstone bridge of the amplifier (Intro-710, WPI) before impalements.

### BODIPY-prazosin staining of α1-adrenergic receptors in the arterial wall

Freshly dissected arteries were loaded for 90 min at room temperature (in the dark) in PSS containing 100 nM BODIPY®-FL-prazosin (B-7433, Life Technologies) in a humidified chamber gassed with 5 % $CO_2$ in air. After loading, the arteries were washed with PSS and mounted on slides for imaging with a LSM 5 Pascal confocal microscope (Zeiss) using a×40 water immersion lens. BODIPY-prazosin was excited by 488 nm argon laser and emitted light between 505 and 530 nm recorded. The pinhole, gain, and laser excitation settings remained constant for all the experiments. A Z-stack (1 μm image steps) was constructed in several locations of the artery wall. A corresponding differential interference contrast image was made for each section.

Data were analyzed by localizing the internal elastic lamina (autofluorescence) in the Z-stack and analyzing the Z-image 4 μm above this (denoted SMC-IL). In a similar fashion, a Z-stack image 4 μm under the adventitia border was analyzed (denoted SMC-OL). The average area analyzed for each image was 15,555 $\mu m^2$. Each artery was analyzed in several locations to provide a single average value for SMC-IL and SMC-OL. Control experiments performed with pre-incubation with 1 μM prazosin for 30 min prior to incubation with 100 nM BODIPY-prazosin confirmed specificity of binding to α1-adrenoceptors (data not shown).

### Solutions and chemicals

The PBS for tissue isolation in immunohistochemical studies contained the following (in mM): 137 NaCl, 2.7 KCl, 8.2 $Na_2HPO_4$, and 1.8 $KH_2PO_4$, at pH 7.4. The PSS for myograph studies contained the following (in mM): 119 NaCl, 4.7 KCl, 1.18 $KH_2PO_4$, 1.17 $MgSO_4$, 25 $NaHCO_3$, 1.6 $CaCl_2$, 0.026 EDTA, and 5.5 glucose, gassed with 5 % $CO_2$ in air and adjusted to pH 7.4. In solutions with increased $K^+$ concentration, NaCl was substituted with equimolar KCl.

Complete Mini, EDTA-free protease inhibitor cocktail was supplied from Roche Applied Science (Germany). Charybdotoxin was purchased from Latoxan (France). All other chemicals were purchased from Sigma Aldrich (Denmark).

### Data analysis

All data are presented as mean values±SEM. Differences between means were tested by one-way ANOVA followed by Bonferroni posttest or by *t* test where appropriate. $P<0.05$ was considered significant and *n* refers to the number of rats.

## Results

### Two splice variants of *Tmem16a* are expressed in rat mesenteric small arteries and in aorta

Fragments of two splice variants of *Tmem16a* were amplified from cDNA prepared from rat mesenteric artery RNA. Subsequent sequencing confirmed these fragments to be a part of *Tmem16a* gene product. Mesenteric small arteries expressed "bc" (deletion of exon 15) or "cd" (deletion of exon 6b) splice variants in accordance with the nomenclature suggested previously [11] (Fig. 1). The primers spanning segment "a" did not amplify any PCR product. Amplification and sequencing of cDNA from rat aorta identified the same two splice variants (not shown).

### In vivo transfection of rat mesenteric small arteries with *Tmem16a*-siRNA downregulates the expression of TMEM16A

Successful downregulation of *Tmem16a* 3 days after transfection with *Tmem16a*-siRNA targeting exon 23 was confirmed at the mRNA level. *Tmem16a* mRNA was significantly reduced by *Tmem16a*-directed siRNA in comparison with the controls: nontransfected arteries, arteries transfected with mutated *Tmem16a*-siRNA, and arteries transfected with eGFP-targeted siRNA (Fig. 2a). No significant difference in *Tmem16a* expression was found

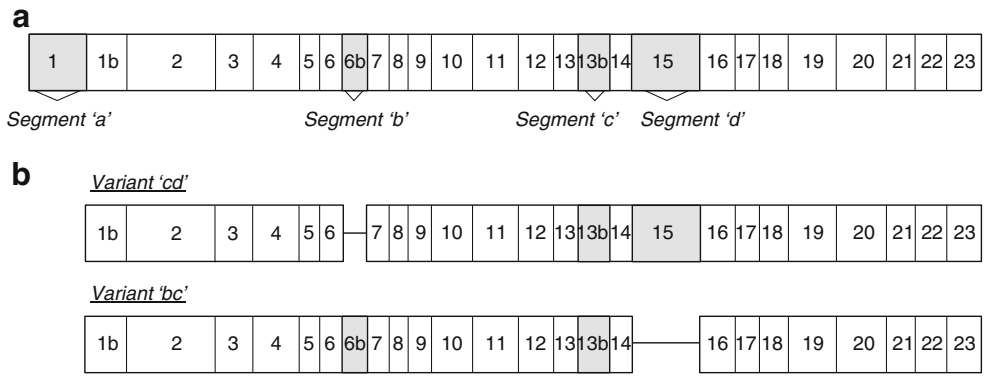


**Fig. 1** Splice variants of *Tmem16a* expressed in rat mesenteric small arteries. **a** Predicted exon structure of rat *Tmem16a*. Exons corresponding to fragments "a," "b," "c," and "d" [11, 12] are indicated. **b** Splice variants found in rat mesenteric small arteries are presented. These splice variants omit either exon 6b or exon 15 corresponding to "b" or "d" fragments of the protein, respectively. Segment "a" was not detected and all variants contained segment "c"

between nontransfected control and arteries transfected either with mutated siRNA or with eGFP-siRNA.

When *Tmem16a*-siRNA-2—which targets another exon (exon 22)—was used for arterial transfection, *Tmem16a* mRNA was also significantly reduced (24.9±5.3 % of the level in nontransfected arteries; $P=0.012$, $n=4$) in comparison with eGFP-target siRNA-transfected arteries (117.0±18.6 %).

The effectiveness of transfection was also validated at the protein level using immunoreactivity against TMEM16A in freshly isolated SMCs (Fig. 2b, c). There was no significant difference in TMEM16A protein expression between SMCs isolated from arteries transfected with eGFP-targeted siRNA and nontransfected arteries. Transfection with *Tmem16a*-siRNA significantly reduced TMEM16A protein expression in comparison with SMCs isolated from arteries transfected with eGFP-targeted siRNA (Fig. 2b).

Downregulation of TMEM16A suppressed also mRNA expression of bestrophin-1 (26.4±10.9 vs. 90.8±8.1 % in eGFP-siRNA-transfected arteries, $P=0.009$, $n=4$), bestrophin-2 (75.8±6.1 vs. 105.5±5.5 %, $P=0.04$, $n=3$), and bestrophin-3 (14.7±5.5 vs. 101.8±15.5 %, $P=0.002$, $n=5$).

## TMEM16A downregulation suppresses $Ca^{2+}$-activated $Cl^-$ currents in smooth muscle cells

In accordance with previous reports [25–27, 37], SMCs freshly isolated from arteries transfected with nonrelated siRNA expressed two $Ca^{2+}$-activated $Cl^-$ conductances, the "classical," niflumic acid-sensitive $I_{Cl(Ca)}$ and the cGMP-dependent, $Zn^{2+}$-sensitive $I_{Cl(Ca)}$ (Fig. 3). SMCs dialyzed with intracellular solution containing 900 nM free $Ca^{2+}$ had a voltage- and time-dependent current which was significantly suppressed by 100 μM niflumic acid (Fig. 3a, b). The biophysical and pharmacological characteristics of this niflumic acid-sensitive $I_{Cl(Ca)}$ are indistinguishable from those previously described for the "classical" $I_{Cl(Ca)}$ [25–27]. The addition of 8Br-cGMP, a membrane-permeable analog of cGMP, in the presence of niflumic acid elicited a second voltage- and time-independent current, which was inhibited by 10 μM $Zn^{2+}$ (Fig. 3a, b). This current corresponds to the cGMP-dependent, $Zn^{2+}$-sensitive $I_{Cl(Ca)}$ (Fig. 3c) characterized previously [25–27].

SMCs isolated from the arteries transfected with nonrelated siRNA had $Ca^{2+}$-activated $Cl^-$ conductances similar to those in nontransfected SMCs. There was no significant difference in the niflumic acid-sensitive $I_{Cl(Ca)}$ or the $Zn^{2+}$-sensitive $I_{Cl(Ca)}$ recorded from these two types of SMCs (data not shown). Both of these $I_{Cl(Ca)}$ were, however, significantly diminished by TMEM16A downregulation (Fig. 3a–c). The whole-cell slope conductances of the niflumic acid-sensitive $I_{Cl(Ca)}$ and the $Zn^{2+}$-sensitive $I_{Cl(Ca)}$ were significantly reduced in SMCs downregulated for TMEM16A in comparison with the control (Fig. 3c).

## TMEM16A downregulation suppresses NA-induced contraction in vivo and inhibits diameter oscillations

There was no difference between diameters of fully relaxed arteries (passive diameters) either transfected with eGFP-targeted siRNA or downregulated for TMEM16A (Fig. 4a). Nonstimulated arteries of both groups had similar basal tone in vivo before NA was applied (12±5 vs. 21±6 % for eGFP-siRNA transfected and downregulated for TMEM16A arteries, respectively; $n=5$). NA constricted eGFP-siRNA in a concentration-dependent manner ($-\log EC_{50}$ was 6.32±0.16, $n=5$; Fig. 4a, b). Arteries downregulated for TMEM16A have small responses to NA (Fig. 4a, c).

All arteries transfected with siRNA-targeted eGFP ($n=5$) produced rhythmic oscillations in the inner diameter when stimulated with NA (Fig. 4b, d). Two out of seven arteries downregulated for TMEM16A did not oscillate in diameter in

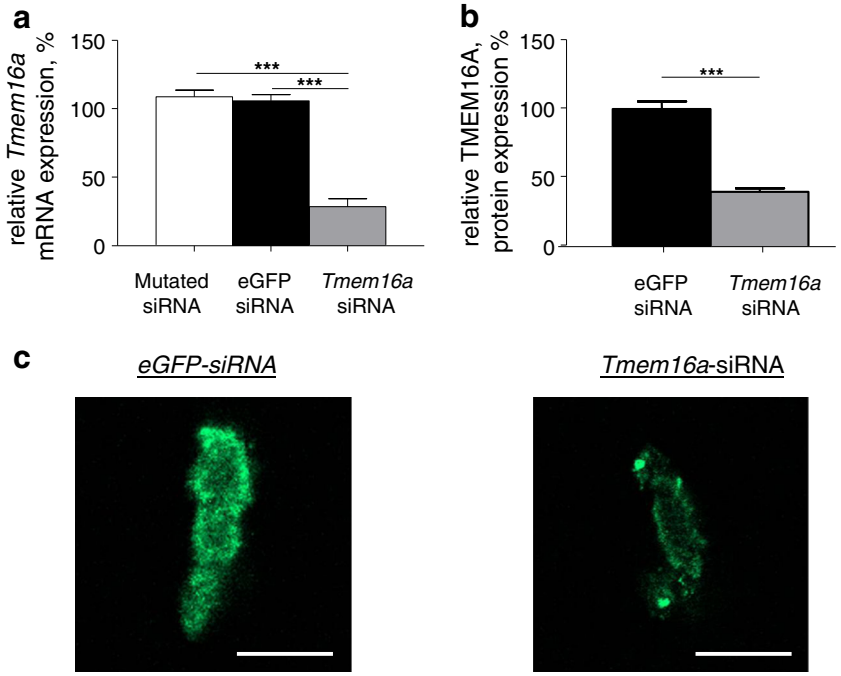


**Fig. 2** Downregulation of *Tmem16a* expression by in vivo transfection of mesenteric small arteries with siRNA directed against *Tmem16a* (*Tmem16a*-siRNA). **a** Relative level of *Tmem16a* mRNA expression in arteries transfected with *Tmem16a*-siRNA, with mutated form of *Tmem16a*-siRNA (mutated siRNA) or siRNA directed against eGFP (eGFP-siRNA). *Tmem16a* expression was normalized to two housekeeping genes, GAPDH and TFRC, and was set to 100 % in nontransfected arteries isolated from the same rat. $n=6$, $^{***}P<0.01$. **b** TMEM16A protein expression (quantified by immunofluorescence) was significantly reduced in SMCs isolated from arteries transfected with *Tmem16a*-siRNA in comparison with SMCs transfected with nonrelated siRNA. Results averaged from 43 to 69 cells isolated from eGFP-siRNA and *Tmem16a*-siRNA-transfected arteries (paired) from three rats; $^{***}P<0.01$. **c** Representative examples for the experiments shown in **b**. SMCs were isolated from mesenteric small arteries segments transfected with eGFP-siRNA (*left panel*) and *Tmem16a*-siRNA (*right panel*) and stained with TMEM16A antibody. Fluorescence of cells incubated with only secondary antibody and without primary antibody was set as a background. The same settings were used for all recordings. *Bars* indicate 20 μm

the presence of NA. The remaining five TMEM16A-downregulated arteries oscillated irregularly and with significantly reduced amplitude (Fig. 4c, d).

## TMEM16A contributes to the agonist-induced contraction of isolated mesenteric small arteries in vitro

Passive inner diameters were not different between the groups of isolated arteries in vitro (Table 2). When active wall tension was compared, the arteries downregulated for TMEM16A had reduced agonist-induced contraction in comparison with nontransfected arteries and arteries transfected with nonfunctional siRNA (Fig. 5). Thus, NA concentration–response curves indicated a significantly reduced sensitivity to the agonist and suppressed maximal contractile responses in TMEM16A-downregulated isolated arteries (Fig. 5a, b; Table 2). Surprisingly, arteries transfected with mutated, nonfunctional siRNA were more sensitive to NA in comparison with nontransfected arteries (Table 2). This was not a consequence of the transfection procedure since the contractile responses of eGFP-siRNA-transfected isolated arteries were not different from the responses of nontransfected isolated arteries (Fig. 5c; Table 2).

Transfection with another *Tmem16a*-siRNA-2 had functional consequences similar to those with *Tmem16a*-siRNA. Thus, *Tmem16a*-siRNA-2 transfection significantly ($P=0.008$) suppressed contractile responses to 30 μM NA—3.82±0.45, 3.51±0.14, and 1.98±0.36 N/m ($n=4$)—for nontransfected arteries, arteries transfected with eGFP-siRNA, and with *Tmem16a*-siRNA-2, respectively.

Elevation of the extracellular $K^+$ concentration (20 mM) potentiated the contractile responses to NA in all three experimental groups but did not modify the difference between the responses of the groups (Fig. 6). Thus, isolated arteries transfected with *Tmem16a*-siRNA were still less sensitive to NA with a reduced maximal contractile response to NA in comparison with both nontransfected arteries and arteries transfected with nonfunctional siRNA (Fig. 6; Table 2).

The maximal contractile response to AVP was also reduced in isolated arteries transfected with *Tmem16a*-siRNA in comparison with nontransfected arteries and the arteries

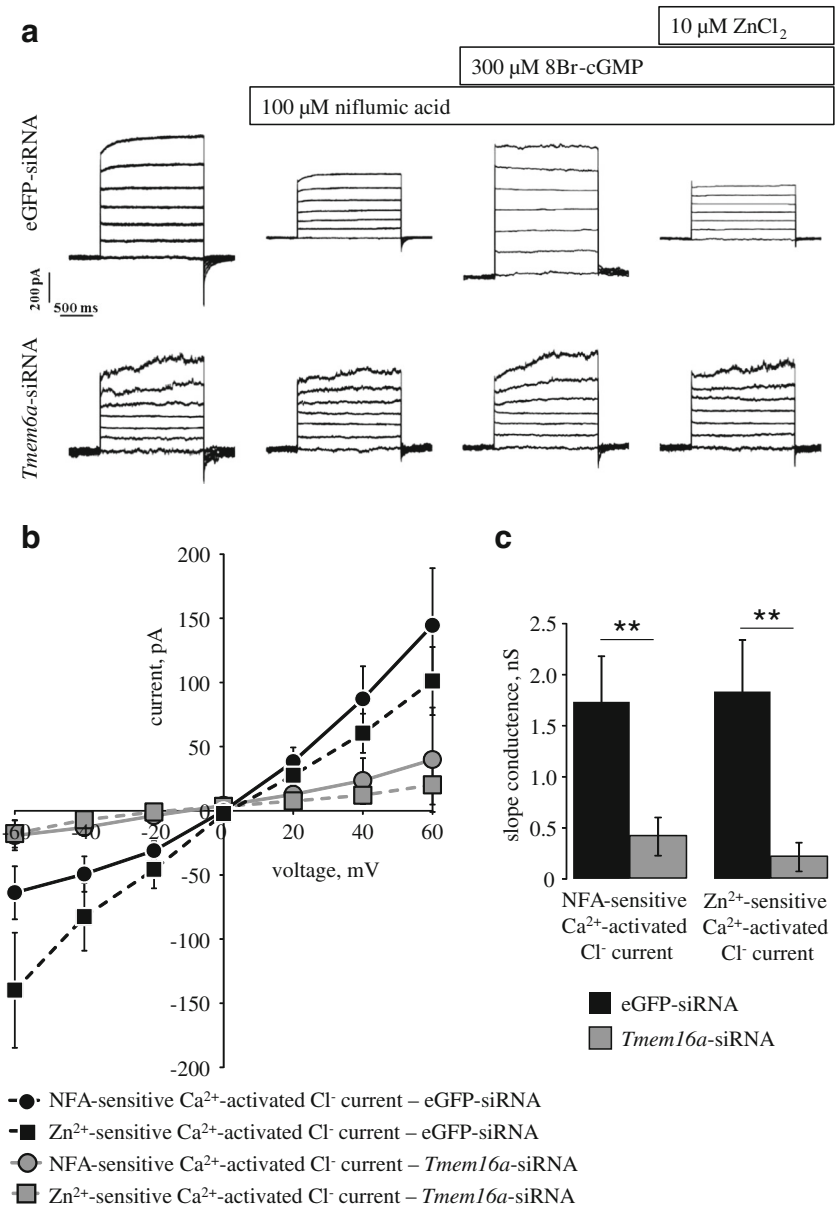


**Fig. 3** TMEM16A downregulation suppresses both the niflumic acid-sensitive and the $Zn^{2+}$-sensitive $Ca^{2+}$-activated $Cl^-$ currents in SMCs isolated from rat mesenteric small arteries transfected with *Tmem16a*-siRNA in vivo. **a** Representative recordings from SMCs transfected with siRNA directed against eGFP (eGFP-siRNA) or with *Tmem16a*-siRNA. Membrane currents were recorded by stepping holding voltage between −60 and +60 mV with 20 mV increments. Membrane currents were consequently recorded under control conditions, after incubation with 100 μM niflumic acid, 300 μM 8Br-cGMP, and 10 μM $ZnCl_2$, as indicated. **b** Averaged current–voltage characteristics for the niflumic acid (NFA)-sensitive and the $Zn^{2+}$-sensitive $Ca^{2+}$-activated $Cl^-$ currents calculated from the experiments similar to those shown in **a**. **c** The whole-cell slope conductances (between −20 and +20 mV) of two currents in **b** measured in SMCs transfected with either siRNA directed against eGFP (eGFP-siRNA) or with *Tmem16a*-siRNA. $n=9$–13; $^{**}P<0.01$

transfected with nonfunctional siRNA: although no significant difference in sensitivity to AVP between arteries transfected with *Tmem16a*-siRNA and nontransfected arteries was observed (Fig. 7). Similar to NA-stimulated arteries, the arteries transfected with mutated nonfunctional siRNA were more sensitive to AVP than nontransfected and TMEM16A-downregulated arteries (Fig. 7a; Table 2). The transfection with eGFP-siRNA did not affect contractile responses to AVP or agonist sensitivity when compared with nontransfected arteries (Fig. 7c).

The contractile response to 124 mM $K^+$ in the presence of 1 μM phentolamine was significantly reduced in isolated arteries transfected with *Tmem16a*-siRNA in comparison with nontransfected arteries and arteries transfected with mutated *Tmem16a*-siRNA (Table 2). The response to $K^+$ depolarization was also significantly reduced ($P=0.008$) in arteries transfected with *Tmem16a*-siRNA-2 (1.21±0.23 N/m, $n=4$) in comparison with nontransfected arteries (2.47±0.40 N/m) and arteries transfected with eGFP-siRNA (2.48±0.28 N/m).

In contrast, the contractile responses to 10 mM caffeine, to evoke release of $Ca^{2+}$ from caffeine-sensitive intracellular stores, were not different between the groups. Both *Tmem16a*-siRNA (Table 2) and *Tmem16a*-siRNA-2 (0.39±0.08, 0.39±0.07, and 0.36±0.06 N/m for nontransfected, transfected with eGFP-siRNA, and *Tmem16a*-siRNA-2

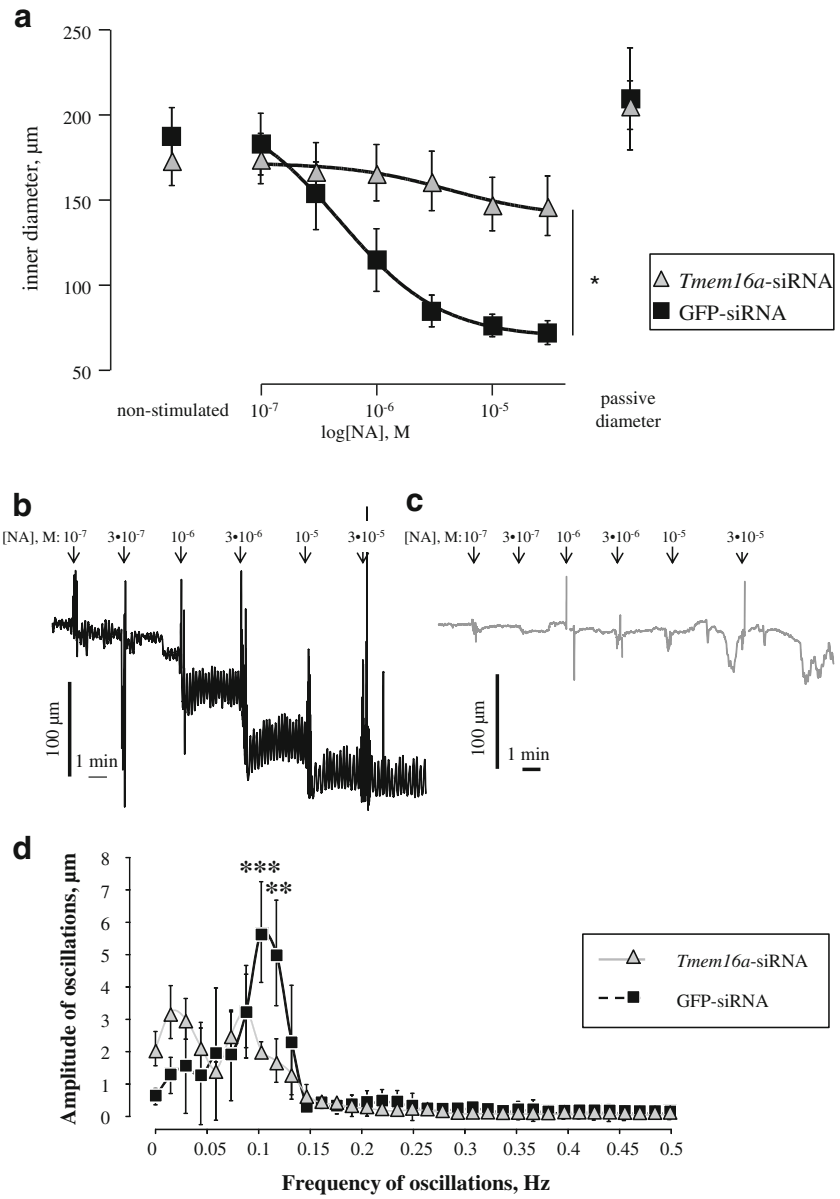


**Fig. 4** Mesenteric small arteries in vivo respond to exogenous NA with changes in arterial inner diameter: matched eGFP-siRNA and *Tmem16a*-siRNA-transfected arteries from the same rat were compared. **a** Averaged inner diameters of arteries transfected with eGFP-siRNA and *Tmem16a*-siRNA and their changes in response to NA. $n=7$, $^*P<0.05$. Representative curves showing the inner diameter changes in response to NA of eGFP-siRNA-transfected artery (**b**) and *Tmem16a*-siRNA-transfected artery in vivo (**c**). **d** The distribution of vasomotion amplitudes over oscillation frequencies 0–0.5 Hz for eGFP-siRNA-transfected arteries ($n=7$) and *Tmem16a*-siRNA-transfected arteries in vivo (two out of seven arteries did not oscillate and were therefore not included in the analysis; $n=5$). $^*P<0.05$

arteries, respectively; $n=4$) transfections had no effect on caffeine-induced contraction. No difference in relaxation to 10 μM acetylcholine was found between the groups, suggesting that endothelial function was unaffected by the transfections (Table 2).

## Reduced membrane depolarization in TMEM16A-downregulated arteries

No difference in the resting membrane potentials of SMCs in arteries transfected with eGFP-siRNA and TMEM16A-downregulated arteries was found (Fig. 8). NA stimulation depolarized the SMCs in both groups; however, the NA-induced depolarization was significantly reduced in TMEM16A-downregulated arteries compared with eGFP-siRNA-transfected arteries (Fig. 8). In contrast, elevation of extracellular $K^+$ to 60 mM equally depolarized the membrane potential in TMEM16A-downregulated arteries and eGFP-siRNA-transfected arteries. Interestingly, while the SMCs in these arteries produced a similar depolarization to $K^+$, the TMEM16A-downregulated arteries still had a reduced contractile response in comparison with eGFP-siRNA-transfected arteries (Fig. 8). The contractile response to $K^+$-induced depolarization was completely blocked by 10 μM nifedipine in all experimental groups (data not shown).

**Table 2** Functional characteristics of arteries in isometric experiments. In one group of experiments, we compared three different groups of arteries from the same rats: *Tmem16a*-siRNA-transfected arteries, arteries transfected with mutated siRNA, and nontransfected arteries. In other experiments, only eGFP-transfected arteries and nontransfected arteries from the same rats were compared

| | Rats transfected with *Tmem16a*-siRNA and mutated siRNA ($n=7$) | | | Rats transfected with eGFP-siRNA ($n=3$) | |
|---|---|---|---|---|---|
| | Nontransfected | *Tmem16a*-siRNA | Mutated siRNA | Nontransfected | eGFP-siRNA |
| ID (μm) | 297±5 | 305±10 | 295±11 | 303±11 | 297±7 |
| $-\log EC_{50}$ NA | 5.68±0.07 | 5.27±0.06***,### | 6.024±0.04** | 5.87±0.08 | 5.82±0.14 |
| $-\log EC_{50}$ AVP | 4.99±0.10 | 4.93±0.09# | 5.20±0.07* | 5.12±0.05 | 5.07±0.10 |
| $-\log EC_{50}$ NA+20 mM $K^+$ | 5.91±0.06 | 5.72±0.11*,### | 6.32±0.08** | | |
| Max NA, N/m | 5.88±0.40 | 2.03±0.50***,## | 4.72±0.48 | 4.81±0.70 | 4.82±0.97 |
| NA+20 mM $K^+$, N/m | 5.70±0.40 | 2.20±0.45***,# | 4.00±0.46 | | |
| Max AVP, N/m | 5.16±0.25 | 3.36±0.44*,# | 5.73±0.55 | 4.86±0.61 | 4.99±0.79 |
| Max $K^+$, N/m | 5.40±0.42 | 2.36±0.44**,# | 4.20±0.55 | | |
| Caffeine, N/m | 0.70±0.10 | 0.60±0.06 | 0.76±0.11 | | |
| Relaxation to ACh, % | 68.01±5.41 | 65.09±6.17 | 63.18±5.41 | 62.11±5.12 | 65.75±5.21 |

*ID* inner diameter, *NA* noradrenaline, *AVP* arginine vasopressin, *ACh* acetylcholine

*$P<0.05$, **$P<0.01$, ***$P<0.001$ vs. nontransfected arteries; #$P<0.05$, ##$P<0.01$, ###$P<0.001$ vs. arteries transfected with mutated, nonfunctional siRNA

### TMEM16A downregulation does not affect the expression of α1-adrenergic receptors

The mRNA levels of different isoforms of α1-adrenergic receptors expressed in the arterial wall of rat mesenteric small arteries were not affected by *Tmem16a*-siRNA transfection and were not significantly different from those in arteries transfected with eGFP-siRNA (Fig. 9a). The localization of α1-adrenergic receptors with BODIPY-prazosin staining (Fig. 9b, c) did not reveal any significant difference in the intensity of staining between nontransfected arteries and arteries transfected with eGFP-siRNA and *Tmem16a*-siRNA.

### Nonselective cationic current is unaffected by TMEM16A downregulation

Intracellular injection of the G-protein activator GTPγS in freshly isolated SMCs uncouples the activation of G-proteins from agonist receptor stimulation and induces a nonselective cationic membrane current ($I_{NSC}$). The $I_{NSC}$ reached a peak 3–7 min after breaking the patch membrane and the SMC dialyzed with GTPγS in the whole-cell voltage-clamp configuration (Fig. 10a). This $I_{NSC}$ was sensitive to nonselective inhibition with micromolar application of $GdCl_3$. There was no significant difference between current–voltage dependencies of GTPγS-evoked $I_{NSC}$ in SMCs isolated from nontransfected arteries and arteries transfected with either eGFP-siRNA or *Tmem16a*-siRNA (Fig. 10b).

### NA-induced $[Ca^2]_i^+$ increase is reduced in TMEM16A-downregulated arteries

TMEM16A-downregulated arteries had suppressed $[Ca^{2+}]_i$ changes in response to NA stimulation in comparison with eGFP-siRNA-transfected arteries (Fig. 11a). The slopes of the relation between NA-induced contraction and $[Ca^{2+}]_i$ increase were not different between the groups indicating that $Ca^{2+}$ sensitivity was not affected (Fig. 11b). In contrast, the increase of $[Ca^{2+}]_i$ following release of $Ca^{2+}$ from the sarcoplasmic reticulum with 10 mM caffeine was similar in all experimental groups (Fig. 11c).

The $[Ca^{2+}]_i$ increase in response to elevated extracellular $K^+$ was significantly reduced in TMEM16A-downregulated arteries in comparison with eGFP-siRNA-transfected arteries (Fig. 11c). The mRNA levels for the vascular L-type calcium channel (*cacna1c*, $Ca_V1.2$) in TMEM16A-downregulated arteries were reduced to 46 % of those in nontransfected arteries (Fig. 11d). No significant changes in *cacna1c* expression were detected in eGFP-siRNA-transfected arteries.

### Vasomotion in vitro is suppressed in TMEM16A-downregulated arteries

Arteries stimulated with NA to develop about 50 % of their maximal tone produce vasomotion (Fig. 12). A single TMEM16A-downregulated artery (out of seven) failed to develop oscillations. The amplitude of vasomotion in the six

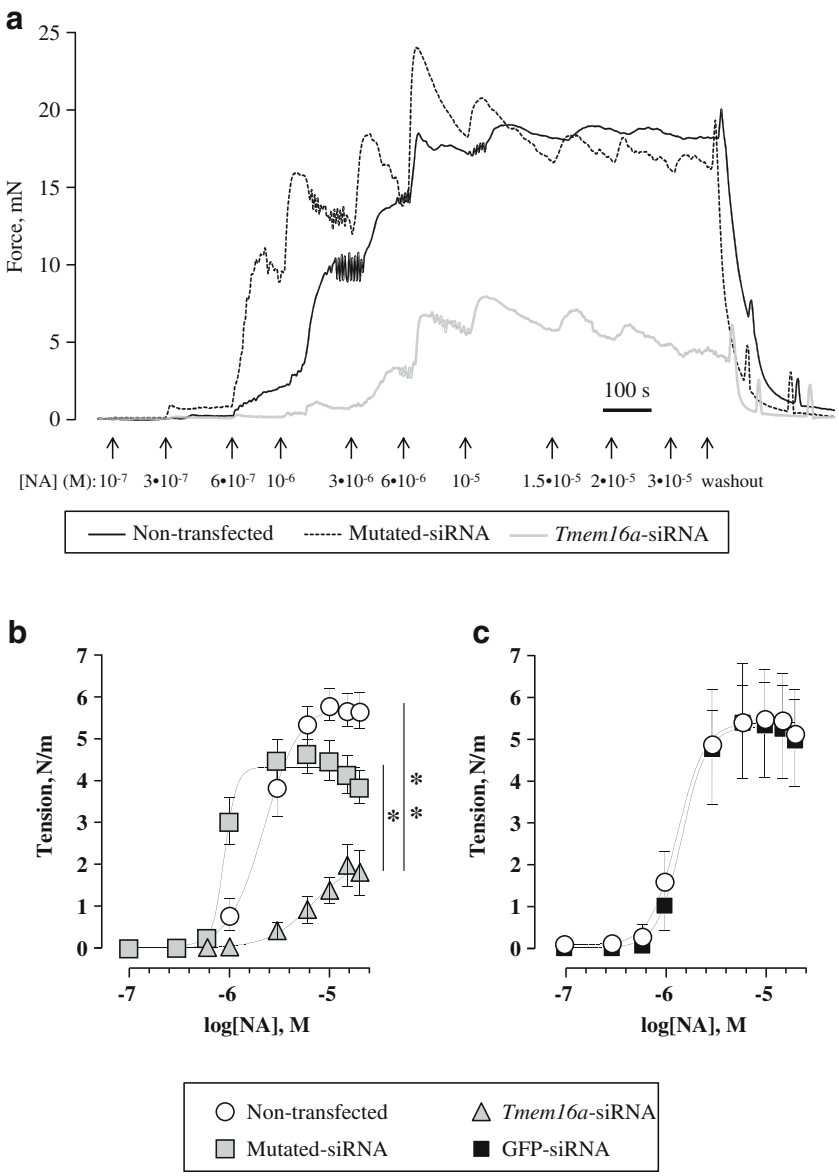


**Fig. 5** Downregulation of TMEM16A suppressed NA-induced contractile response of isolated rat mesenteric arteries in vitro. **a** Representative trace for NA concentration–response experiment. **b** Concentration–response to NA of TMEM16A-downregulated arteries, arteries transfected with mutated siRNA, and nontransfected arteries ($n=7$). **c** NA concentration–contraction relations of eGFP-siRNA-transfected and nontransfected arteries in vitro ($n=3$). *$P<0.05$, **$P<0.01$

TMEM16A-downregulated arteries displaying oscillations was significantly reduced in comparison with nontransfected arteries, arteries transfected with mutated siRNA, and siRNA directed against eGFP (Fig. 12). The transfection procedure itself did not apparently alter vasomotion, since no significant difference between vasomotion amplitude and frequency was found in the three control groups of arteries.

## Discussion

We find in this study that the expression of TMEM16A is necessary for the two $I_{Cl(Ca)}$ present in vascular SMC. Moreover, we have found that TMEM16A is an important modulator of agonist-induced contraction and vasomotion in rat mesenteric small arteries in vivo and in vitro. Knockdown of TMEM16A with siRNA reduces arterial contraction in two potential ways: via reduced depolarization— as might be expected for reduction of a vascular $Cl^-$ channel—and, surprisingly, via reduction of voltage-gated $Ca^{2+}$ channel expression in the SMC.

### TMEM16A as the SMC CaCC

We have previously demonstrated that vascular SMCs have two $Ca^{2+}$-activated $Cl^-$ conductances [26]: the "classical" $I_{Cl(Ca)}$ and the cGMP-dependent $I_{Cl(Ca)}$ with distinct pharmacological and biophysical properties [25, 27, 38, 39]. Downregulation of TMEM16A (confirmed at both mRNA and protein levels) caused the classical $I_{Cl(Ca)}$ to disappear

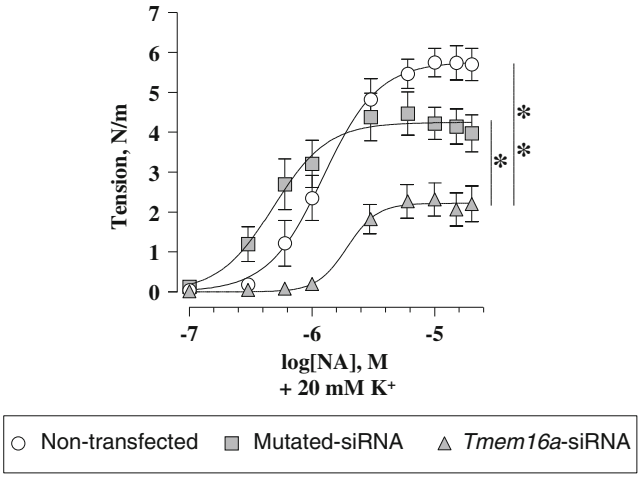


**Fig. 6** NA-induced contractile response in the presence of 20 mM $K^+$ was suppressed in TMEM16A-downregulated isolated rat mesenteric arteries in comparison with the arteries transfected with nonfunctional siRNA and with nontransfected arteries ($n=7$). *$P<0.05$, **$P<0.01$

from SMCs: consistent with previous data where the niflumic acid-sensitive $I_{Cl(Ca)}$ was significantly reduced by ex vivo TMEM16A downregulation in SMCs from pulmonary [24] and cerebral arteries [4, 44, 46]. These findings taken together with the predominant near membrane localization of TMEM16A seen here and the previous suggestions of TMEM16A as CaCC [5, 47] provide strong evidence that TMEM16A constitutes the "classical" $I_{Cl(Ca)}$ in SMCs of mesenteric small arteries.

Unexpectedly, downregulation of TMEM16A also led to disappearance of the cGMP-dependent $I_{Cl(Ca)}$. Importantly, this was accompanied by downregulation in bestrophin-1, bestrophin-2, and bestrophin3 mRNA, indicating that bestrophin mRNA regulation is influenced by TMEM16A expression. We have previously seen that specific downregulation of bestrophin-3 also downregulates bestrophin-1 and bestrophin-2 in SMCs [27], making it difficult to distinguish between whether TMEM16A directly

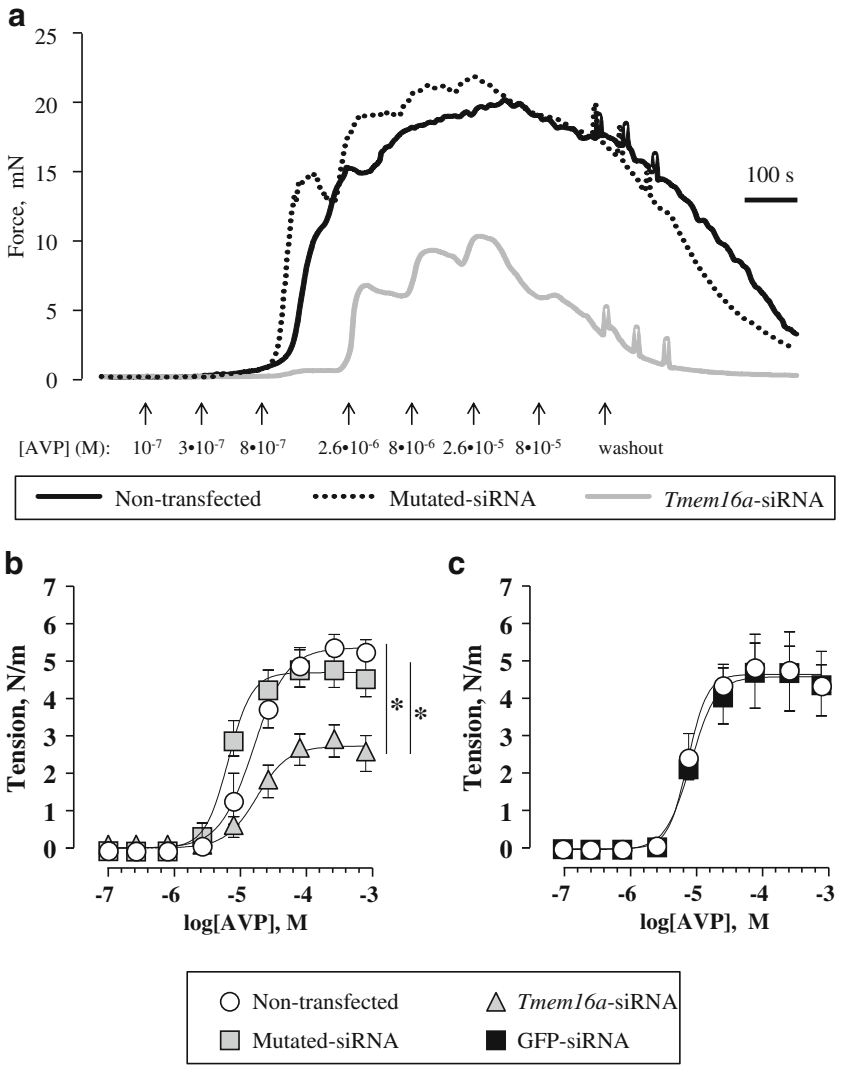


**Fig. 7** Downregulation of TMEM16A reduced AVP-induced contractile responses of isolated rat mesenteric small arteries in vitro. **a** Representative trace of a concentration–response curve for AVP. **b** Concentration–response relations for AVP of TMEM16A-downregulated arteries, arteries transfected with nonfunctional siRNA, and nontransfected arteries ($n=7$). *$P<0.05$. **c** Concentration–response relations for AVP of eGFP-siRNA-transfected and nontransfected arteries ($n=3$)

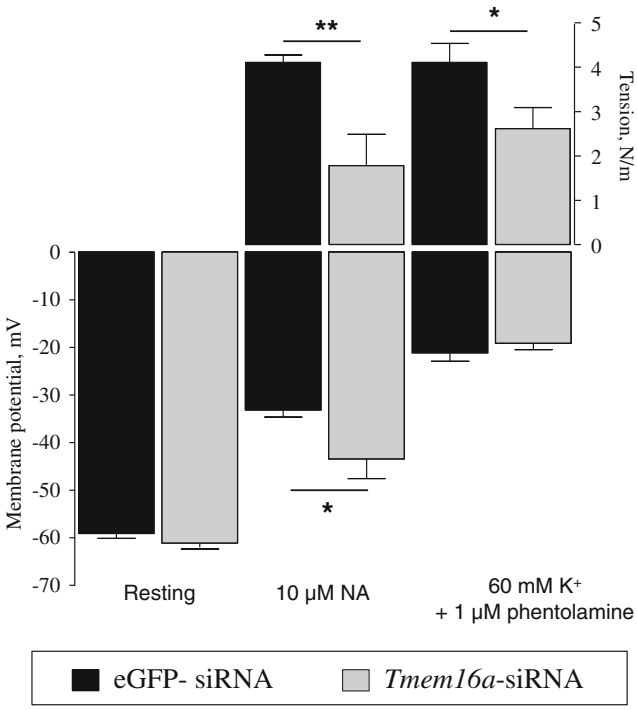


**Fig. 8** TMEM16A-downregulated arteries can depolarize to the same extent as eGFP-siRNA-transfected arteries but they have reduced contractility. Membrane depolarization to NA and tone production in *Tmem16a*-siRNA arteries was lower in comparison with eGFP-siRNA-transfected arteries. Resting membrane potential and depolarization to 60 mM $K^+$ were unchanged, but force production to elevated extracellular $K^+$ is also lower in *Tmem16a*-siRNA arteries compared to eGFP-siRNA arteries ($n$=6–7). *$P$<0.05, **$P$<0.01

controls the expression of all three bestrophins or TMEM16A regulates one of them, which secondarily leads to downregulation of the others.

Based on these findings, we suggest two possible models for interaction between TMEM16A and bestrophins. One possibility is that one bestrophin (or their combination) forms the channel responsible for the cGMP-dependent $I_{Cl(Ca)}$ and that TMEM16A through regulation of bestrophin expression is important for this current. Another possibility is that the TMEM16A protein alone forms the channel pore for both $Ca^{2+}$-activated $Cl^-$ conductances, while accessory subunits (e.g., bestrophins) impart the biophysical and pharmacological characteristics of cGMP-dependent $I_{Cl(Ca)}$ conducted by TMEM16A. Bestrophins have previously been suggested to interact with TMEM16A [1] similar to the functional and molecular interaction between the cystic fibrosis transmembrane regulator (CFTR) and TMEM16A [33]. Future studies will determine the nature of these interactions.

A potentially important factor contributing to the variability of a CaCC protein's physical properties is the expression of different splice variants. We found two splice variants of TMEM16A in the blood vessels: rat aorta and mesenteric small arteries express the splice variant "bc" and "cd." We were unable to find products containing segment "a, " while all products contained segment "c," which is important for voltage sensitivity [11]. Although the functional significance of segment "d" is unknown, segment "b" has been suggested to modulate the $Ca^{2+}$ sensitivity of the TMEM16A-associated CaCC [11].

## TMEM16A and vascular function

In contrast to our expectations, the mutated (four mismatching nucleotides) *Tmem16a*-siRNA significantly potentiated agonist-induced contraction. The cause of this effect is not clear: no changes in TMEM16A expression or $Cl^-$ currents were seen after transfection with mutated *Tmem16a*-siRNA. Rat mesenteric arteries typically display an increased sensitivity to agonist(s) and increased maximal response if the endothelium has been removed [10] or is poorly functioning; however, we did not find any difference in the endothelium-derived relaxation elicited by acetylcholine between the artery groups. While this effect may not be attributable to an endothelial defect, it is nevertheless an off-target effect of the mutated siRNA since transfection with nonrelated eGFP-siRNA was without effect on arterial contractility.

We found decreased contractile responses to NA and AVP in the isolated arteries downregulated for TMEM16A. To elucidate the mechanism for this, we made an in-depth investigation of the possible factors involved in the reduced response to NA. Our findings that the NA-induced depolarization and increase of $[Ca^{2+}]_i$ were reduced are consistent with CaCCs being important for membrane depolarization and force development [7, 18, 19, 21, 34–36, 41] and the observation that CaCCs can be activated by G-protein-coupled receptor stimulation [9, 19, 34, 45]. Our findings are also consistent with a recent report of TMEM16A in the cerebral vascular bed, where the pressure-induced depolarization and development of myogenic tone were reduced when TMEM16A was knocked down ex vivo [4]. Furthermore, since the increase of $[Ca^{2+}]_i$ and force development to caffeine were identical in the two groups, it seems unlikely that $Ca^{2+}$ release and/or alterations in the contractile proteins are contributing to the reduced agonist-induced contraction.

However, full substitution of $Cl^-$ with aspartate and dissipation of the elevated intracellular $Cl^-$ inhibits all $I_{Cl(Ca)}$ but is without substantial effect on the sensitivity or maximal contraction to NA [2, 31]. Also downregulation of bestrophin, which inhibits the cGMP-dependent $I_{Cl(Ca)}$, does not affect the response to NA [3]. Finally, the few studies that have tested the effect on the membrane potential of the $Cl^-$ gradient in NA-activated arteries have detected only a minimal effect [2, 31]. We therefore assessed whether other parameters of

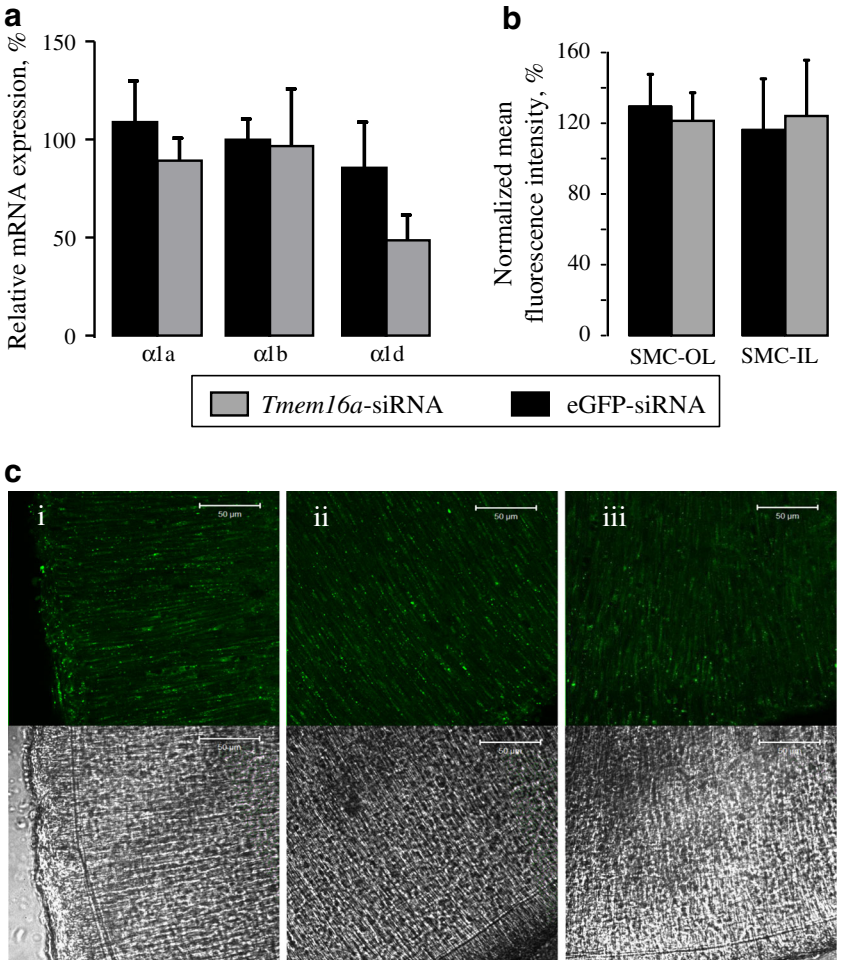


**Fig. 9** Downregulation of TMEM16A does not affect the expression of α1-adrenergic receptors. **a** Relative mRNA level of α1a, α1b, and α1d isoforms of adrenergic receptors in arteries transfected with either *Tmem16a*-siRNA or siRNA directed against eGFP (eGFP-siRNA). *Tmem16a* expression was set to 100 % in nontransfected arteries isolated from the same rat. $n=4$. No significant difference between the groups was found. **b** The average intensity of BODIPY-prazosin staining (representative images in **c**) in the SMCs of the outer layer of the media (SMC-OL) and the inner layer (SMC-IL) normalized to the intensity observed in the nontransfected artery (set to 100 %). No significant difference between nontransfected arteries and arteries transfected with either *Tmem16a*-siRNA or eGFP-siRNA was found. **c** Representative BODIPY-prazosin staining of *Tmem16a*-siRNA-transfected arteries (*i*), eGFP-siRNA-transfected arteries (*ii*), and nontransfected arteries (*iii*) for BODIPY-prazosin staining and corresponding differential interference contrast image for the same artery. *Scale bar* represents 50 μm in all images

importance for NA-induced depolarization and force development were affected. To evaluate an effect on α1-adrenoceptor expression, we measured α1-receptor mRNA and fluorescent prazosin binding but found neither to be affected by downregulation of TMEM16A. We also measured stimulated cation unspecific current which participates in NA-induced depolarization, but again found no difference in arteries downregulated for TMEM16A.

An indication that other pathways may be affected came from the highly surprising finding that TMEM16A downregulation also reduces force development to high extracellular $K^+$. To provide mechanistic insight to this, we measured membrane potential and $[Ca^{2+}]_i$ with high extracellular $K^+$. While the membrane potential was similar, $[Ca^{2+}]_i$ was lower in the arteries where TMEM16A was downregulated. The latter finding supports and provides an explanation for the reduced force development. These findings could be explained by reduction of L-type $Ca^{2+}$ channel expression and/or function in the SMCs: to test this possibility, we measured mRNA expression of the pore-forming subunit of the L-type voltage-gated $Ca^{2+}$ channel and found a significant reduction. The mechanism responsible for this effect of siRNA directed against TMEM16A is as yet unclear, but this finding suggests a complicated functional role for TMEM16A in vascular tissues. It seems possible that TMEM16A acts as a multifunctional protein, similar to CFTR, being a CaCC in its own right as well as an important regulator of other

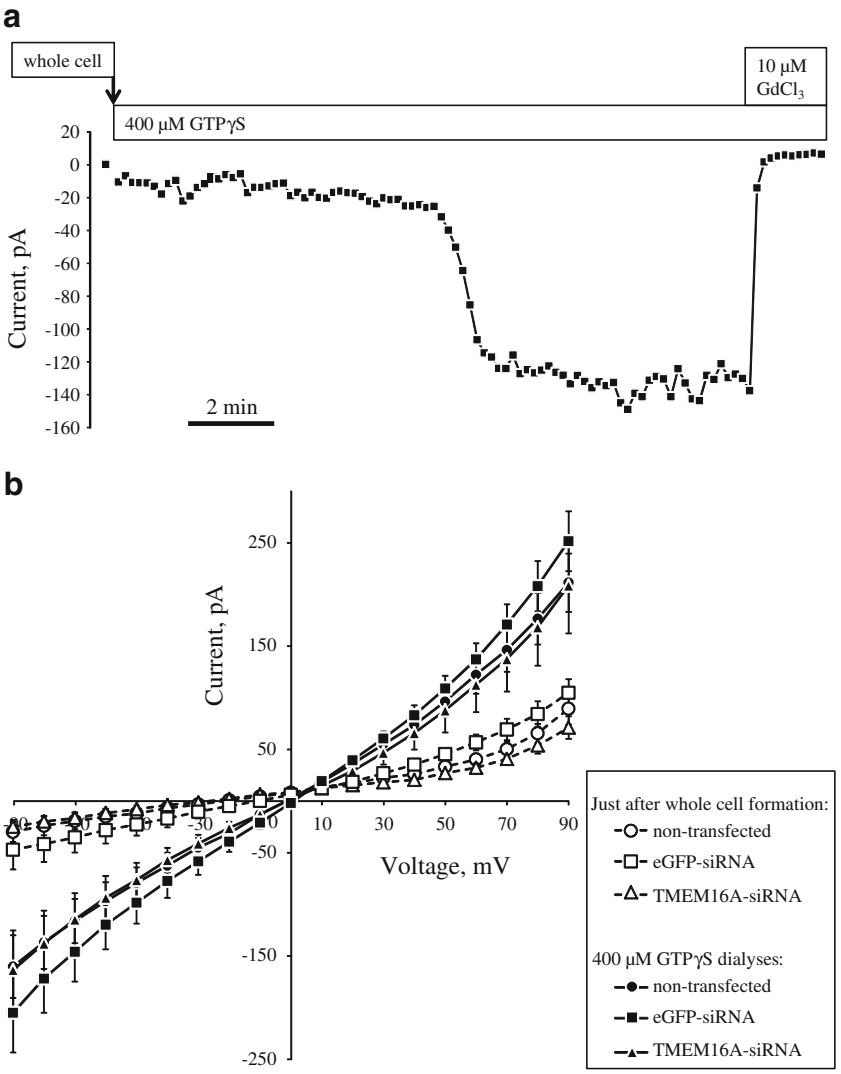


**Fig. 10** Downregulation of TMEM16A has no effect on nonselective cation current ($I_{NSC}$). $I_{NSC}$ was evoked by dialyses of isolated SMCs with 400 μM GTPγS from the patch pipette. SMCs were held at −50 mV and the GTPγS-evoked $I_{NSC}$ current reached a peak 3 to 7 min after breakthrough to the whole-cell configuration (indicated by an *arrow* in **a**). This $I_{NSC}$ was inhibited by 10 μM $GdCl_3$. **a** Representative current trace at holding potential −50 mV recorded on SMC isolated from an artery transfected with *Tmem16a*-siRNA. **b** The averaged current–voltage relationships for baseline membrane currents recorded immediately after breaking through the patch membrane and the peak $I_{NSC}$ recorded in SMCs isolated from nontransfected arteries ($n=6$), arteries transfected with eGFP-siRNA ($n=6$), and arteries transfected with *Tmem16a*-siRNA ($n=8$)

ion channels, such as the L-type $Ca^{2+}$ channels [30]. The extent to which TMEM16A modulates agonist-induced contraction directly by providing depolarizing current and indirectly as a modulator of $Ca^{2+}$ channels is unclear. We suggest, however, that both these mechanisms may play a role. Interestingly, bestrophin-1 has previously been shown to change the properties of voltage-gated $Ca^{2+}$ channels [42, 48] and could therefore be suggested as a link between $Ca^{2+}$ channels and TMEM16A although our previous study where we downregulated bestrophins in the vascular wall does not support this possibility as there was no effect on arterial contractility [3].

## TMEM16A is important for the generation of vasomotion

We have previously suggested that the cGMP-dependent $I_{Cl(Ca)}$ is important for synchronization of vascular SMCs during rat mesenteric artery vasomotion [37]. We have recently supported this hypothesis by demonstrating that downregulation of the bestrophins and consequently cGMP-dependent $I_{Cl(Ca)}$ [27] suppresses the amplitude of vasomotion without affecting the frequency [3]. The current study provides additional evidence for this by showing that suppression of the cGMP-dependent $I_{Cl(Ca)}$ by downregulation of TMEM16A also reduced vasomotion amplitude. We have shown that vasomotion, which is well characterized in vitro, is also present in rat mesenteric artery in vivo. Importantly, the prevalence and coordination of vasomotion in vivo were significantly reduced by TMEM16A downregulation. Although the membrane of TMEM16A downregulated arteries depolarized less to NA (to∼−45 mV) compared to the control (∼−35 mV), which in itself could influence the ability of the membrane potential to oscillate, we have previously shown that rat mesenteric small arteries do oscillate around both potentials [2, 29].

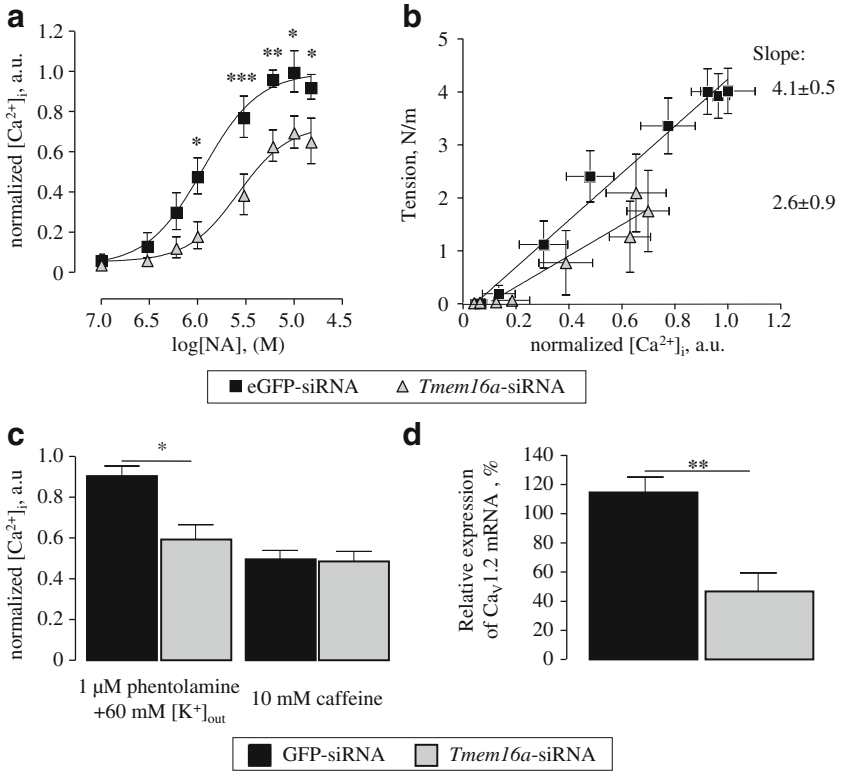


**Fig. 11** Downregulation of TMEM16A suppresses intracellular $Ca^{2+}$ ($[Ca^{2+}]_i$) rises in response to NA and $K^+$, partly as a consequence of reduced expression of vascular L-type calcium channel ($Ca_V1.2$). **a** Changes in $[Ca^{2+}]_i$ in response to increasing concentration of NA. $[Ca^{2+}]_i$ signaling is normalized to averaged maximal $[Ca^{2+}]_i$ level obtained in arteries transfected with eGFP-siRNA after 10 μM NA stimulation ($n=6$). $^*P<0.05$, $^{**}P<0.01$, $^{***}P<0.001$. **b** $Ca^{2+}$ sensitivity expressed as a relation between wall tension and normalized $[Ca^{2+}]_i$, as shown in **a** ($n=6$). **c** Changes in $[Ca^{2+}]_i$, in response to 60 mM $K^+$-induced depolarization and 10 mM caffeine stimulation. $[Ca^{2+}]_i$ signaling is normalized to averaged maximal $[Ca^{2+}]_i$ level in arteries transfected with eGFP-siRNA after 10 μM NA stimulation ($n=6$). $^*P<0.05$. **d** Expression of $Ca_V1.2$ in TMEM16A-downregulated arteries and eGFP-siRNA-transfected arteries ($n=6$). $^{**}P<0.01$

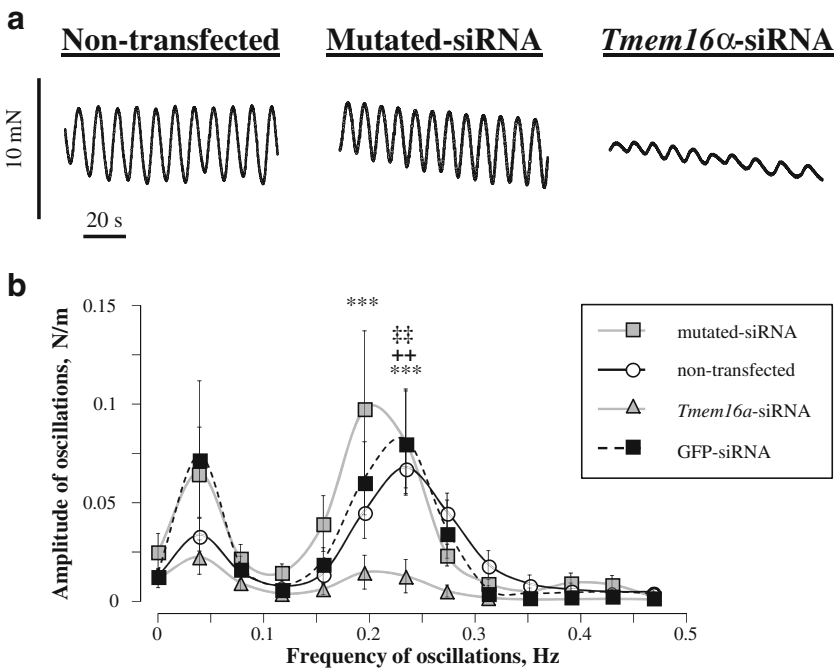


**Fig. 12** Downregulation of TMEM16A reduced the amplitude but not the frequency of NA-induced vasomotion in isolated rat mesenteric small arteries in vitro. **a** Representative recordings of NA-induced vasomotion in nontransfected and TMEM16A-downregulated arteries. **b** The distribution of vasomotion amplitudes over oscillation frequencies 0–0.5 Hz. $^{***}P<0.001$ for arteries transfected with mutated siRNA ($n=6$) vs. TMEM16A-downregulated arteries ($n=6$). $^{++}P<0.01$ for nontransfected arteries ($n=9$) vs. TMEM16A-downregulated arteries. $^{‡‡}P<0.01$ for eGFP-siRNA transfected arteries ($n=3$) vs. TMEM16A-downregulated arteries

## Conclusion

The present study clearly demonstrates the expression and functional significance of TMEM16A in SMCs in rat mesenteric small arteries. Expression of TMEM16A was necessary for two biophysically and pharmacologically different $Ca^{2+}$-activated $Cl^-$ currents in vascular SMCs. TMEM16A was found to be important for vasomotion: this effect is likely at least in part due to the concurrent loss of the cGMP component of $Ca^{2+}$-activated $Cl^-$ conductance in SMCs. Interestingly, downregulation of TMEM16A was followed by a reduction of agonist-induced contraction, which is associated with a reduction of $[Ca^{2+}]_i$ and may only in part be explained by reduced depolarization. At the same depolarized potential (with high $K^+$), $[Ca^{2+}]_i$ was also reduced in TMEM16A-downregulated arteries, which intriguingly might be explained by altered L-type $Ca^{2+}$ channel expression as we observe reduced mRNA for this channel. Further studies are necessary to clarify how and to what extent TMEM16A expression affects other transmembrane proteins and/or ion channels.

**Acknowledgments** We thank Jane Holbæk Rønn, Jørgen Andresen, Viola Smed Mose Larsen, and Sukhan Kim for excellent technical assistance. The study was supported by the Danish Research Council, the Lundbeck Foundation, and the Novo Nordisk Foundation.



## Reference

1. Barro-Soria R, Aldehni F, Almaca J, Witzgall R, Schreiber R, Kunzelmann K (2010) ER-localized bestrophin 1 activates $Ca^{2+}$-dependent ion channels TMEM16A and SK4 possibly by acting as a counterion channel. Pflugers Arch 459:485–497
2. Boedtkjer DM, Matchkov VV, Boedtkjer E, Nilsson H, Aalkjaer C (2008) Vasomotion has chloride-dependency in rat mesenteric small arteries. Pflugers Arch 457:389–404
3. Broegger T, Jacobsen JC, Secher DV, Boedtkjer DM, Kold-Petersen H, Pedersen FS, Aalkjaer C, Matchkov VV (2011) Bestrophin is important for the rhythmic but not the tonic contraction in rat mesenteric small arteries. Cardiovasc Res 91:685–693
4. Bulley S, Neeb ZP, Burris SK, Bannister JP, Thomas-Gatewood CM, Jangsangthong W, Jaggar JH (2012) TMEM16A channels contribute to the myogenic response in cerebral arteries. Circ Res 111:1027–1036
5. Caputo A, Caci E, Ferrera L, Pedemonte N, Barsanti C, Sondo E, Pfeffer U, Ravazzolo R, Zegarra-Moran O, Galietta LJ (2008) TMEM16A, a membrane protein associated with calcium-dependent chloride channel activity. Science 322:590–594
6. Chipperfield AR, Harper AA (2000) Chloride in smooth muscle. Prog Biophys Mol Biol 74:175–221
7. Criddle DN, de Moura RS, Greenwood IA, Large WA (1996) Effect of niflumic acid on noradrenaline-induced contractions of the rat aorta. Br J Pharmacol 118:1065–1071
8. Davis AJ, Forrest AS, Jepps TA, Valencik ML, Wiwchar M, Singer CA, Sones WR, Greenwood IA, Leblanc N (2010) Expression profile and protein translation of TMEM16A in murine smooth muscle. Am J Physiol 299:C948–C959
9. Elble RC, Ji G, Nehrke K, DeBiasio J, Kingsley PD, Kotlikoff MI, Pauli BU (2002) Molecular and functional characterization of a murine calcium-activated chloride channel expressed in smooth muscle. J Biol Chem 277:18586–18591
10. Falloon BJ, Stephens N, Tulip JR, Heagerty AM (1995) Comparison of small artery sensitivity and morphology in pressurized and wire-mounted preparations. Am J Physiol 268:H670–H678
11. Ferrera L, Caputo A, Ubby I, Bussani E, Zegarra-Moran O, Ravazzolo R, Pagani F, Galietta LJ (2009) Regulation of TMEM16A chloride channel properties by alternative splicing. J Biol Chem 284:33360–33368
12. Ferrera L, Scudieri P, Sondo E, Caputo A, Caci E, Zegarra-Moran O, Ravazzolo R, Galietta LJ (2011) A minimal isoform of the TMEM16A protein associated with chloride channel activity. Biochim Biophys Acta 1808:2214–2223
13. Galietta LJ (2009) The TMEM16 protein family: a new class of chloride channels? Biophys J 97:3047–3053
14. Greenwood IA, Leblanc N (2007) Overlapping pharmacology of $Ca^{2+}$-activated $Cl^-$ and $K^+$ channels. Trends Pharmacol Sci 28:1–5
15. Hartzell C, Putzier I, Arreola J (2005) Calcium-activated chloride channels. Annu Rev Physiol 67:719–758
16. Hartzell HC (2008) Physiology CaCl-ing channels get the last laugh. Science 322:534–535
17. Huang F, Rock JR, Harfe BD, Cheng T, Huang X, Jan YN, Jan LY (2009) Studies on expression and function of the TMEM16A calcium-activated chloride channel. Proc Natl Acad Sci U S A 106: 21413–21418
18. Janssen LJ, Sims SM (1992) Acetylcholine activates non-selective cation and chloride conductances in canine and guinea-pig tracheal myocytes. J Physiol 453:197–218
19. Kirkup AJ, Edwards G, Green ME, Miller M, Walker SD, Weston AH (1996) Modulation of membrane currents and mechanical activity by niflumic acid in rat vascular smooth muscle. Eur J Pharmacol 317:165–174
20. Kunzelmann K, Tian Y, Martins JR, Faria D, Kongsuphol P, Ousingsawat J, Thevenod F, Roussa E, Rock J, Schreiber R (2011) Anoctamins. Pflugers Arch 462:195–208
21. Lamb FS, Kooy NW, Lewis SJ (2000) Role of Cl(−) channels in alpha-adrenoceptor-mediated vasoconstriction in the anesthetized rat. Eur J Pharmacol 401:403–412
22. Large WA, Wang Q (1996) Characteristics and physiological role of the $Ca^{2+}$-activated $Cl^-$ conductance in smooth muscle. Am J Physiol 271:C435–C454
23. Leblanc N, Ledoux J, Saleh S, Sanguinetti A, Angermann J, O'Driscoll K, Britton F, Perrino BA, Greenwood IA (2005) Regulation of calcium-activated chloride channels in smooth muscle cells: a complex picture is emerging. Can J Physiol Pharmacol 83: 541–556
24. Manoury B, Tamuleviciute A, Tammaro P (2010) TMEM16A/anoctamin 1 protein mediates calcium-activated chloride currents in pulmonary arterial smooth muscle cells. J Physiol 588:2305–2314
25. Matchkov VV, Aalkjaer C, Nilsson H (2004) A cyclic GMP-dependent calcium-activated chloride current in smooth-muscle cells from rat mesenteric resistance arteries. J Gen Physiol 123:121–134
26. Matchkov VV, Aalkjaer C, Nilsson H (2005) Distribution of cGMP-dependent and cGMP-independent $Ca^{2+}$-activated $Cl^-$ conductances in smooth muscle cells from different vascular beds and colon. Pflugers Arch 451:371–379
27. Matchkov VV, Larsen P, Bouzinova EV, Rojek A, Boedtkjer DM, Golubinskaya V, Pedersen FS, Aalkjaer C, Nilsson H (2008) Bestrophin-3 (vitelliform macular dystrophy 2-like 3 protein) is

essential for the cGMP-dependent calcium-activated chloride conductance in vascular smooth muscle cells. Circ Res 103:864–872
28. Matchkov VV, Moeller-Nielsen N, Secher DV, Nourian Z, Bodtkjer DM, Aalkjaer C (2012) The alpha2 isoform of the Na,K-pump is important for intercellular communication, agonist-induced contraction and EDHF-like response in rat mesenteric arteries. Am J Physiol 303:H36–H46
29. Matchkov VV, Rahman A, Bakker LM, Griffith TM, Nilsson H, Aalkjaer C (2006) Analysis of effects of connexin-mimetic peptides in rat mesenteric small arteries. Am J Physiol 291:H357–H367
30. Mehta A (2005) CFTR: more than just a chloride channel. Pediatr Pulmonol 39:292–298
31. Nilsson H, Videbaek LM, Toma C, Mulvany MJ (1998) Role of intracellular calcium for noradrenaline-induced depolarization in rat mesenteric small arteries. J Vasc Res 35:36–44
32. Okamoto H, Unno T, Arima D, Suzuki M, Yan HD, Matsuyama H, Nishimura M, Komori S (2004) Phospholipase C involvement in activation of the muscarinic receptor-operated cationic current in guinea pig ileal smooth muscle cells. J Pharmacol Sci 95:203–213
33. Ousingsawat J, Kongsuphol P, Schreiber R, Kunzelmann K (2011) CFTR and TMEM16A are separate but functionally related Cl channels. Cell Physiol Biochem 28:715–724
34. Pacaud P, Loirand G, Baron A, Mironneau C, Mironneau J (1991) $Ca^{2+}$ channel activation and membrane depolarization mediated by $Cl^-$ channels in response to noradrenaline in vascular myocytes. Br J Pharmacol 104:1000–1006
35. Pacaud P, Loirand G, Gregoire G, Mironneau C, Mironneau J (1992) Calcium-dependence of the calcium-activated chloride current in smooth muscle cells of rat portal vein. Pflugers Arch 421:125–130
36. Parai K, Tabrizchi R (2002) A comparative study of the effects of $Cl^-$ channel blockers on mesenteric vascular conductance in anaesthetized rat. Eur J Pharmacol 448:59–66
37. Peng H, Matchkov V, Ivarsen A, Aalkjaer C, Nilsson H (2001) Hypothesis for the initiation of vasomotion. Circ Res 88:810–815
38. Piper AS, Large WA (2004) Direct effect of $Ca^{2+}$/calmodulin on cGMP-activated $Ca^{2+}$-dependent $Cl^-$ channels in rat mesenteric artery myocytes. J Physiol 559:449–457
39. Piper AS, Large WA (2004) Single cGMP-activated $Ca^{2+}$-dependent $Cl^-$ channels in rat mesenteric artery smooth muscle cells. J Physiol 555:397–408
40. Pusch M (2004) $Ca^{2+}$-activated chloride channels go molecular. J Gen Physiol 123:323–325
41. Remillard CV, Lupien MA, Crepeau V, Leblanc N (2000) Role of $Ca^{2+}$- and swelling-activated $Cl^-$ channels in alpha1-adrenoceptor-mediated tone in pressurized rabbit mesenteric arterioles. Cardiovasc Res 46:557–568
42. Rosenthal R, Bakall B, Kinnick T, Peachey N, Wimmers S, Wadelius C, Marmorstein A, Strauss O (2006) Expression of bestrophin-1, the product of the VMD2 gene, modulates voltage-dependent $Ca^{2+}$ channels in retinal pigment epithelial cells. FASEB J 20:178–180
43. Schroeder BC, Cheng T, Jan YN, Jan LY (2008) Expression cloning of TMEM16A as a calcium-activated chloride channel subunit. Cell 134:1019–1029
44. Thomas-Gatewood C, Neeb ZP, Bulley S, Adebiyi A, Bannister JP, Leo MD, Jaggar JH (2011) TMEM16A channels generate Ca(2)-activated Cl currents in cerebral artery smooth muscle cells. Am J Physiol 301:H1819–H1827
45. Van Renterghem C, Lazdunski M (1993) Endothelin and vasopressin activate low conductance chloride channels in aortic smooth muscle cells. Pflugers Arch 425:156–163
46. Wang M, Yang H, Zheng LY, Zhang Z, Tang YB, Wang GL, Du YH, Lv XF, Liu J, Zhou JG, Guan YY (2012) Downregulation of TMEM16A calcium-activated chloride channel contributes to cerebrovascular remodeling during hypertension through promoting basilar smooth muscle cell proliferation. Circulation 125:697–707
47. Yang YD, Cho H, Koo JY, Tak MH, Cho Y, Shim WS, Park SP, Lee J, Lee B, Kim BM, Raouf R, Shin YK, Oh U (2008) TMEM16A confers receptor-activated calcium-dependent chloride conductance. Nature 455:1210–1215
48. Yu K, Xiao Q, Cui G, Lee A, Hartzell HC (2008) The best disease-linked Cl−channel hBest1 regulates Ca V 1 (L-type) $Ca^{2+}$ channels via src-homology-binding domains. J Neurosci 28:5660–5670